

Slowly rotating super-compact Schwarzschild stars

Camilo Posada-Aguirre,¹★

¹*Department of Physics and Astronomy, University of South Carolina, 712 Main Street, Columbia SC, 29208 USA*

ABSTRACT

The Schwarzschild interior solution, or ‘Schwarzschild star’, which describes a spherically symmetric homogeneous mass with constant energy density, shows a divergence in pressure when the radius of the star reaches the Buchdahl-Bondi bound. Recently Mazur and Mottola showed that this divergence is integrable through the Komar formula, inducing non-isotropic transverse stresses on a surface of some radius R_0 . When this radius approaches the Schwarzschild radius $R_s = 2M$, the interior solution becomes one of negative pressure evoking a de Sitter spacetime. This gravitational condensate star, or gravastar, is an alternative solution to the idea of a black hole as the ultimate state of gravitational collapse. Using Hartle’s model to calculate equilibrium configurations of slowly rotating masses, we report results of surface and integral properties for a Schwarzschild star in the very little studied region $R_s < R < (9/8)R_s$. We found that in the gravastar limit, the angular velocity of the fluid relative to the local inertial frame tends to zero, indicating rigid rotation. Remarkably, the normalized moment of inertia I/MR^2 and the mass quadrupole moment Q approach to the corresponding values for the Kerr metric to second order in Ω . These results provide a solution to the problem of the source of a slowly rotating Kerr black hole.

Key words: Rotating Gravastar, Interior Schwarzschild solution, Hartle’s equations.

1 INTRODUCTION

In classical General Relativity it is commonly accepted that the final state of complete gravitational collapse is a singular state called a ‘black hole’ (Misner et al. 1973; Wald 1984). This object is characterized by a central space-time singularity at $r = 0$ surrounded by an event horizon, a null hypersurface located at the Schwarzschild radius $R_s = 2M$ which separates points connected to infinity by a timelike curve from those that are not. These features are a consequence of the exact solution to Einstein’s field equations in the vacuum found a century ago by Schwarzschild (1916) which describes the exterior space-time geometry of a spherically symmetric mass.

Despite the vast amount of literature [see e.g. (Wald 2001; Page 2005)], the physical reality of the black hole concept has not only generated some skepticism (Abramowicz et al. 2002; Frolov 2014; Hawking 2014), but also has raised some paradoxical issues which have not been consistently solved. A pivotal one is the non-conservation of information by quantum matter falling into a black hole (Hawking 1976). Additionally in the original Hawking (1975) radiation derivation, the backward-in-time propagated mode seems to experience a large blueshift with energies larger than the Planck energy. It is expected that these highly ‘blue-shifted’ photons would leave a non-negligible ‘imprint’ on the spacetime geometry, making the approximation of fixed classical geometry background untenable (Mazur & Mottola 2001; Mottola 2011). Moreover, the arbi-

trarily large values of entropy at $T_H \rightarrow 0$ associated with the black hole as predicted by the Bekenstein (1974) formula in the classical limit $\hbar \rightarrow 0$ produces serious challenges to the foundations of quantum mechanics. It is believed that the resolution of these issues will be achieved in the framework of a consistent theory of quantum gravity. We still do not possess such a theory, therefore it is valuable to investigate alternative solutions to the aforementioned problems.

Alternatives have been introduced to alleviate some of the black hole paradoxes (Stephens et al. 1994; Chapline 2001; Berezhin 2003). In particular, we concentrate in the *gravastar* (vacuum condensate gravitational star) model proposed by Mazur & Mottola (2001, 2004). A gravastar is basically the aftermath of a gravitational collapsing star to the Schwarzschild radius R_s , whose final state is characterized by a modified de Sitter interior region with negative pressure and a finite surface tension. The exterior spacetime remains the standard spherically symmetric Schwarzschild exterior solution.

In connection with the gravastar, Mazur & Mottola (2015) considered the constant density Schwarzschild interior solution, or ‘Schwarzschild star’. As it is well known, this interior solution shows a divergence in pressure when the radius of the star $R = (9/4)M$ (Buchdahl 1959). The existence of this limit in addition to the homogeneous mass approximation, considered ‘unrealistic’, have been assumed as sufficient reasons to exclude the Schwarzschild star from further investigation (Wald 1984; Narlikar 2010). This complete disregard of the interior solution, has left the interesting region $R_s < R < (9/8)R_s$ unexplored.

★ Contact e-mail: posadaag@email.sc.edu

In a bold approach [Mazur & Mottola \(2015\)](#) analyzed this ‘forbidden’ region and found that the divergence in the central pressure is integrable through the Komar formula, producing a δ -function of transverse stresses implying a relaxation of the isotropic fluid condition on a surface of some radius R_0 . In the limit when $R \rightarrow R_s^+$ from above and $R_0 \rightarrow R_s^-$ from below, the interior region suffers a phase transition (starting at the center) becoming one of negative pressure evoking a de Sitter spacetime. This non-singular ‘bubble’ of dark energy which is matched to an external vacuum Schwarzschild spacetime, has zero entropy and temperature, so providing a consistent picture of a gravitational Einstein-Bose condensate, or gravastar, as the final state of complete gravitational collapse.

Some authors ([Lobo 2006](#)) have investigated possible sources for the interior of the gravastar, and the electrically charged case was considered by [Horvat et al. \(2009\)](#). The issue of stability against axial perturbations was studied by [Chirenti & Rezzolla \(2007\)](#). They found that gravastars are stable under axial perturbations, moreover, the quasi-normal modes of rotating gravastars deviate from those associated with a black hole. They concluded that this might help to discern observationally between a gravastar and a black hole. Radial and axial gravitational perturbations on thin-shell gravastars were studied by [Pani et al. \(2009\)](#).

Perturbation theory can also be applied to the study of equilibrium configurations of slowly rotating compact objects. In a seminal paper [Hartle \(1967\)](#) provided the relativistic structure equations to determine the equilibrium configurations of slowly rotating stars to second order in the angular velocity. In Hartle’s model the interior of the star is composed of a fluid characterized by a general one-parameter equation of state (EOS). This configuration is matched to a stationary and axially symmetric exterior region across a timelike hypersurface.

[Chandrasekhar & Miller \(1974\)](#) studied slowly rotating homogeneous masses characterized by a constant energy density, using Hartle’s framework. For this configuration they solved numerically the structure equations for several values of the parameter R/R_s , where R is the radius of the star and R_s is the Schwarzschild radius. Using these solutions Chandrasekhar & Miller calculated integral and surface equilibrium properties such as moment of inertia and mass quadrupole moment up to the Buchdahl bound. They found that the ellipticity of the star, considering constant mass and angular momentum, manifests a prominent maximum at the radius $R/R_s \sim 2.4$. One result of particular interest is that for a star with the ‘minimum possible’ radius $R = (9/8)R_s$, the quadrupole mass moment is very close to the value associated with the Kerr metric to second order in the angular velocity.

Motivated by the aforementioned works, in this paper we report results of surface and integral properties for a slowly rotating Schwarzschild star in the unstudied region $R_s < R < (9/8)R_s$. These results extends those presented by [Chandrasekhar & Miller \(1974\)](#) which were considered up to the Buchdahl radius. We show that for a Schwarzschild star in the gravastar limit when $R \rightarrow R_s$, surface properties like moment of inertia, angular velocity and mass quadrupole moment approach to the corresponding Kerr metric values. These remarkable results provide a long sought solution to the problem of the source of rotation of a slowly rotating Kerr black hole. Throughout the paper, we use geometrized units where $c = G = 1$.

2 SCHWARZSCHILD STAR AND GRAVASTAR LIMIT

The Schwarzschild interior solution corresponding to a spherical configuration with constant energy density, is discussed in standard general relativity textbooks (see e.g. [Wald 1984](#); [Narlikar 2010](#)). The starting point is a spherically symmetric spacetime in Schwarzschild coordinates

$$ds^2 = -e^{2\nu(r)} dt^2 + e^{2\lambda(r)} dr^2 + r^2 (d\theta^2 + \sin^2 \theta d\phi^2). \quad (1)$$

The stress-energy tensor for a spherically symmetric fluid is given by

$$T^\mu_\nu = \begin{pmatrix} -\epsilon & 0 & 0 & 0 \\ 0 & p & 0 & 0 \\ 0 & 0 & p_\perp & 0 \\ 0 & 0 & 0 & p_\perp \end{pmatrix} \quad (2)$$

where ϵ , p and p_\perp correspond to the energy density, radial pressure and tangential pressure respectively, which are functions of r only. The energy density ϵ and the pressure p are related through a given one-parameter EOS. The relevant components of the Einstein equation $G^\mu_\nu = 8\pi T^\mu_\nu$, are

$$e^{-2\lambda} \left(2r \frac{d\lambda}{dr} - 1 + e^{2\lambda} \right) = 8\pi \epsilon r^2, \quad (3)$$

$$e^{-2\lambda} \left(2r \frac{d\nu}{dr} + 1 - e^{2\lambda} \right) = 8\pi p r^2, \quad (4)$$

jointly with the energy-momentum conservation relation

$$\nabla_\mu T^\mu_r = \frac{dp}{dr} + (\epsilon + p) \frac{d\nu}{dr} + \frac{2}{r} (p - p_\perp) = 0 \quad (5)$$

which corresponds to the relativistic generalization of the hydrostatic equilibrium equation or Tolman-Oppenheimer-Volkoff (TOV) equation. It is conventional to introduce

$$h(r) \equiv e^{-2\lambda(r)} = 1 - \frac{2m(r)}{r}, \quad (6)$$

where the function $m(r)$ is associated to the mass within a radius r and is given by the Misner-Sharp relation ([Misner et al. 1973](#))

$$m(r) = \int_0^r dr 4\pi r^2 \epsilon. \quad (7)$$

In terms of (7), (4) becomes

$$\frac{d\nu}{dr} = \frac{m(r) + 4\pi p r^3}{r[r - 2m(r)]}, \quad (8)$$

which in the non-relativistic limit reduces to Poisson’s equation $d\nu/dr = m(r)/r^2$, where $\nu(r)$ is associated to the Newtonian gravitational potential. The interior solution, or *Schwarzschild star*, is matched at the boundary $r = R$ to the asymptotically flat vacuum exterior Schwarzschild solution

$$e^{2\nu(r)_{ext}} = h_{ext}(r) = 1 - \frac{2M}{r}, \quad r \geq R \quad (9)$$

where M is the total mass and R is the radius of the star. The functions $p(r)$ and $m(r)$ satisfy the boundary conditions $p(R) = 0$, $m(R) = M$. The interior region is modeled as an incompressible and isotropic fluid $p = p_\perp$ with

$$\epsilon = \bar{\epsilon} = \frac{3M}{4\pi R^3} = \text{const.} \quad (10)$$

It is useful to define ([Mazur & Mottola 2015](#))

$$\epsilon \equiv \frac{3H^2}{8\pi}, \quad H^2 = \frac{R_s}{R^3}, \quad (11)$$

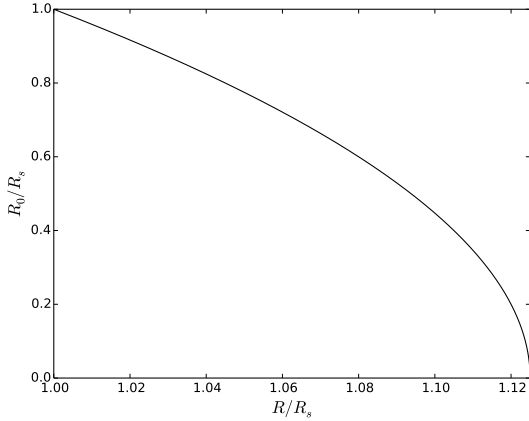


Figure 1. R_0 as a function of R (in units of R_s).

where $R_s = 2M$ is the Schwarzschild radius. In terms of (11), equations (6) and (7) can be solved to obtain

$$m(r) = \frac{4\pi}{3} \bar{\epsilon} r^3 = M \left(\frac{r}{R} \right)^3, \quad h(r) = 1 - H^2 r^2, \quad 0 \leq r \leq R. \quad (12)$$

From (5) the pressure takes the form

$$p(r) = \bar{\epsilon} \left[\frac{\sqrt{1 - H^2 r^2} - \sqrt{1 - H^2 R^2}}{3 \sqrt{1 - H^2 R^2} - \sqrt{1 - H^2 r^2}} \right]. \quad (13)$$

The metric function $e^{2\nu(r)}$ for $r < R$ can be computed to give

$$f(r) \equiv e^{2\nu(r)} = \frac{1}{4} \left[3 \sqrt{1 - H^2 R^2} - \sqrt{1 - H^2 r^2} \right]^2 \geq 0. \quad (14)$$

Across the boundary of the configuration $r = R$, this function must match the exterior metric (9). The continuity of $f(r)$ guarantees that an observer crossing the boundary will not notice any discontinuity of time measurements. Notice that (14) is regular except at some radius R_0 where the denominator in (13)

$$D \equiv 3 \sqrt{1 - H^2 R^2} - \sqrt{1 - H^2 r^2}, \quad (15)$$

vanishes in the range $0 < r < R$. Remarkably, it can be seen from (13) and (14) that the pressure goes to infinity at the same point where $f(r) = 0$. This singular radius can be found directly from (15) to be

$$R_0 = 3R \sqrt{1 - \frac{8}{9} \frac{R}{R_s}}, \quad (16)$$

which is imaginary for $R/R_s > 9/8$. In this regime, $p(r)$ and $f(r)$ are positive. Moreover, when $R \rightarrow (9/8)R_s^+$ from above, (16) shows that R_0 approaches the real axis at $R_0 = 0$ and a divergence of the pressure appears jointly with $f(r) \rightarrow 0$. This limit value $R_B = (9/8)R_s$, or Buchdahl bound (Buchdahl 1959), fixes the maximum possible mass for a star with given radius R . At this radius R_B general relativity predicts that the star cannot remain in static equilibrium. Furthermore, once the star reaches this critical point, its gravitational collapse is inevitable.

Due to the manifestation of this divergence in pressure at the Buchdahl bound, in addition to the incompressible fluid approximation considered artificial (Narlikar 2010), the Schwarzschild star solution below the Buchdahl bound have been ignored in the literature. Mazur & Mottola (2015) in a bold approach, analyzed the region $R_s < R < (9/8)R_s$ and they found that the zero of D given by (16) moves outwards from the origin to finite values $0 < R_0 < R$

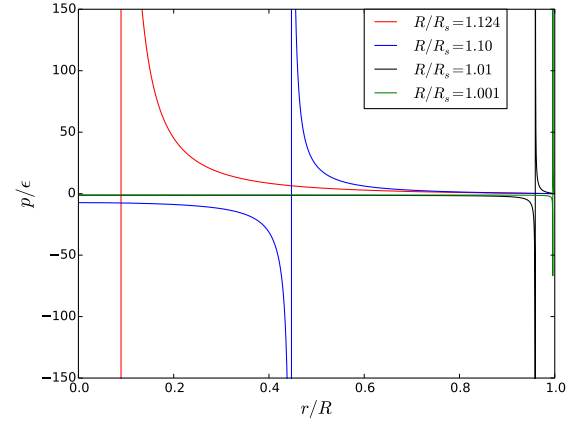


Figure 2. Pressure (in units of ϵ) as a function of r (in units of the star radius R) of the interior Schwarzschild solution for various values of the ratio R/R_s below the Buchdahl bound. Notice the approach of the negative interior pressure $p \rightarrow -\epsilon$ as $R \rightarrow R_s^+$ from above and $R_0 \rightarrow R_s^+$ from below.

(see Fig.1). Then emerges a region where $p(r) < 0$, $f(r) > 0$ and $D < 0$, covering the range $0 \leq r < R_0$. As the radius of the star keeps approaching the Schwarzschild radius from above $R \rightarrow R_s^+$, meanwhile $R_0 \rightarrow R_s^-$ from below, where R_0 is given by (16) which corresponds to the radius of the sphere where the pressure is divergent and $f(R_0) = 0$ (see Fig. 3). Analysis of (13) shows that the new interior region becomes one of *constant negative pressure* $p = -\epsilon$ for $r < R = R_0 = R_s$ (see Fig.2). In this limit, the interior metric function (14) becomes

$$f(r) = \frac{1}{4} (1 - H^2 r^2) = \frac{1}{4} h(r) = \frac{1}{4} \left(1 - \frac{r^2}{R_s^2} \right), \quad H = \frac{1}{R_s} \quad (17)$$

which is a patch of modified de Sitter spacetime. The exterior region $r > R_s$ remains the vacuum spherically symmetric Schwarzschild geometry (9), with an infinitesimal thin shell discontinuity at $R_s = 2M$ where there is a jump in pressure and the zeroes $f = h = 0$ of the interior modified de Sitter and exterior vacuum Schwarzschild match.

Although there is no event horizon, $R = R_s$ is a null hypersurface. However in contrast to the black hole, the gravastar does not require the interior region $r < R_s$ to be a trapped surface. Moreover, the gravastar solution with interior $p = -\epsilon$, has no entropy neither any temperature validating its *condensate state* nature.

Mazur & Mottola (2015) showed that the divergence in pressure at R_0 can be integrated through the Komar formula. However this integration demands that $p_{\perp} \neq p$, therefore breaking the isotropic fluid condition. Below the Buchdahl bound $R < \frac{9}{8}R_s$ the relation for pressure is

$$8\pi \sqrt{\frac{f}{h}} r^2 (p_{\perp} - p) = \frac{8\pi\epsilon}{3} R_0^3 \delta(r - R_0) \quad (18)$$

indicating an anisotropy in pressure at $r = R_0$. It is this δ -function integrable through the Komar formula, together with the relaxation of the isotropic perfect fluid condition at $r = R_0$, which provides a physical interpretation of the Schwarzschild star. The surface energy can be found to be

$$E_s = \frac{8\pi}{3} \epsilon R_0^3 = 2M \left(\frac{R_0}{R_s} \right)^3, \quad (19)$$

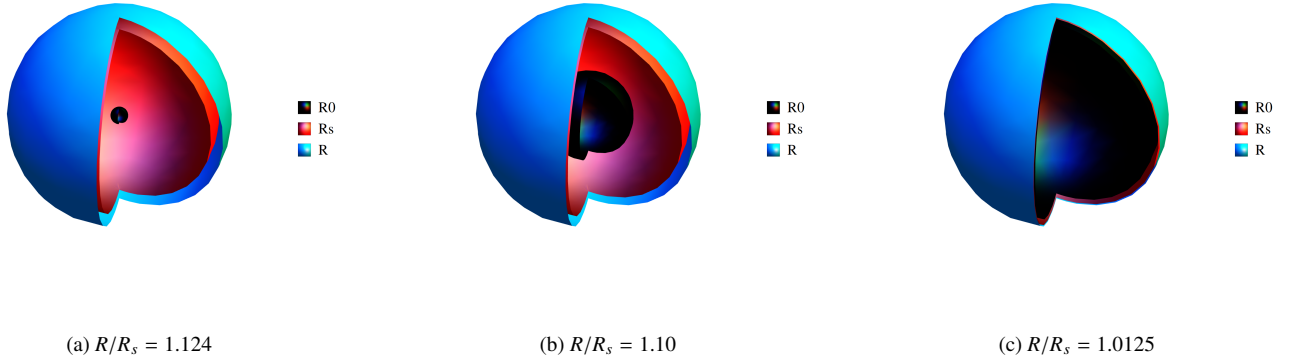


Figure 3. Pictorial diagram of the Schwarzschild star in the regime $R_s < R < (9/8)R_s$, showing the approach of the surface of the star R (Cyan) to the Schwarzschild surface R_s (Red). The radius of the star is measured in units of the Schwarzschild radius R_s . The surface R_0 (Black) where the pressure diverges (and $f = h = 0$) is shown at different stages. Figure 3a, shows that R_0 emerges at the center of the star where the fluid suffers a phase transition. The region $0 \leq r < R_0$ with negative pressure starts approaching R_s from below, meanwhile the radius of the star R approaches R_s from above (see Fig. 3b). In the gravastar limit when $R \rightarrow R_s^+$ and $R_0 \rightarrow R_s^-$, the whole interior region is one of constant negative pressure given by a static patch of modified de Sitter spacetime with a finite surface tension (see Fig. 3c). The exterior spacetime is described by the standard vacuum Schwarzschild metric. Instead of an event horizon, an infinitely thin shell forms at the Schwarzschild radius R_s where there is a jump in pressure and the zeroes $f = h = 0$ of the interior modified de Sitter and exterior Schwarzschild match.

together with the discontinuity on the surface gravities

$$\delta\kappa \equiv \kappa_+ - \kappa_- = \frac{R_s R_0}{R^3} \quad (20)$$

which provides a surface tension at $r = R_0$ given by

$$\tau_s = \frac{MR_0}{4\pi R^3} = \frac{\Delta\kappa}{8\pi G}. \quad (21)$$

In contrast to a black hole, (21) corresponds to a physical surface tension (localized in an infinitesimal thin shell at $r = R_s$) provided by a surface energy and positive transverse pressure as determined by the Komar formula.

Notice that the Schwarzschild star solution provides an instructive limiting case of a stellar model in general relativity. Furthermore, as it was shown by Mazur & Mottola (2015), in the limit when $R \rightarrow R_s^+$ and $R_0 \rightarrow R_s^-$, the Schwarzschild star turns out to be the non-singular gravitational condensate star or *gravastar*, with a surface tension at R_s , proposed by Mazur & Mottola (2001, 2004) as an alternative to black holes as the final state of gravitational collapse.

In the next section we will review the perturbative method developed by Hartle (1967), to study equilibrium configurations of slowly rotating relativistic stars. We will apply these methods to the slowly rotating Schwarzschild star in the, long-time ignored, region $R_s < R < (9/8)R_s$.

3 HARTLE'S STRUCTURE EQUATIONS

In this section the equations of structure for slowly rotating masses derived by Hartle (1967) are summarized. The Hartle model is based on the consideration of an initially static configuration set in slow rotation. In this approximation, changes in pressure, energy density and gravitational field are much less than unity. This condition implies that $R\Omega \ll 1$ where R is the radius of the star and Ω its angular velocity.

The appropriate line element for this situation is ¹

$$ds^2 = -e^{2\nu_0} [1 + 2h_0(r) + 2h_2(r)P_2(\cos\theta)] dt^2 + e^{2\lambda_0} \left\{ 1 + \frac{e^{2\lambda_0}}{r} [2m_0(r) + 2m_2(r)P_2(\cos\theta)] \right\} dr^2 + r^2 [1 + 2k_2(r)P_2(\cos\theta)] \{ d\theta^2 + [d\phi - \omega(r)dt]^2 \sin^2\theta \}, \quad (22)$$

where $P_2(\cos\theta)$ is the Legendre polynomial of order 2; $(h_0, h_2, m_0, m_2, k_2)$ are quantities of order Ω^2 ; and ω , which is proportional to the angular velocity of the star Ω , is a function of r that describes the dragging of the inertial frames. One can introduce a local Zero-Angular-Momentum-Observer (ZAMO) (Stergioulas 2003), then the function $\omega(r)$ corresponds to the angular velocity of the local ZAMO relative to a distant observer. In the non-rotating case the metric (22) reduces to (1).

In the coordinate system of (22), the fluid inside the configuration rotates uniformly with four-velocity u^μ components (Hartle & Thorne 1968)

$$u^\mu = (-g_{tt} - 2\Omega g_{t\phi} - g_{\phi\phi}\Omega^2)^{-1/2} = e^{-\nu_0} \left[1 + \frac{1}{2} r^2 \sin^2\theta (\Omega - \omega)^2 e^{-\nu_0/2} - h_0 - h_2 P_2(\cos\theta) \right], \quad (23)$$

$$u^\phi = \Omega u^t, \quad u^r = u^\theta = 0.$$

It is conventional to define

$$\varpi \equiv \Omega - \omega, \quad (24)$$

to be the angular velocity of the fluid as measured by the local ZAMO. The magnitude of the centrifugal force is determined by this quantity which, at first order in Ω , satisfies the equation

$$\frac{d}{dr} \left(r^4 j(r) \frac{d\varpi}{dr} \right) + 4r^3 \frac{dj}{dr} \varpi = 0, \quad (25)$$

¹ The subscript (0) in the metric functions denotes quantities in the static configuration, except for the functions h_0 and m_0 which corresponds to the first order terms expansions.

with

$$j(r) \equiv e^{-(\lambda_0 + v_0)}. \quad (26)$$

In the exterior empty region $r > R$, $j(r) = 1$ and (25) can be easily integrated to give

$$\varpi(r) = \Omega - \frac{2J}{r^3}, \quad (27)$$

where the constant J corresponds to the angular momentum of the star (Hartle 1967). Equation (25) will be integrated outward from the origin with the boundary conditions $\varpi(0) = \varpi_c = \text{const.}$, and $d\varpi/dr = 0$. The value of ϖ_c is chosen arbitrarily. Once the solution on the surface is found, one can determine the angular momentum J and the angular velocity Ω through the formulas

$$J = \frac{1}{6} R^4 \left(\frac{d\varpi}{dr} \right)_{r=R}, \quad \Omega = \varpi(R) + \frac{2J}{R^3}. \quad (28)$$

The angular momentum is related linearly to Ω through the relation $J = I\Omega$, where I is the relativistic moment of inertia.

Additionally, due to the rotation, the star will deform carrying with it changes in pressure and energy density given by (Hartle & Thorne 1968)

$$p + (\epsilon + p) [\delta p_0 + \delta p_2 P_2(\cos \theta)] \equiv p + \Delta P \quad (29)$$

$$\epsilon + (\epsilon + p) (d\epsilon/dp) [\delta p_0 + \delta p_2 P_2(\cos \theta)] \equiv \epsilon + \Delta \epsilon \quad (30)$$

where δp_0 and δp_2 are functions of r , proportional to Ω^2 , which corresponds to perturbations in pressure and energy density. The spherical deformations can be studied from the $l = 0$ equations with the condition that the central energy density is the same as in the static configuration. The relevant expressions are

$$\frac{dm_0}{dr} = 4\pi r^2 (\epsilon + p) \frac{d\epsilon}{dp} \delta p_0 + \frac{1}{12} r^4 j^2 \left(\frac{d\varpi}{dr} \right)^2 - \frac{1}{3} r^3 \varpi^2 \frac{dj^2}{dr}, \quad (31)$$

$$\frac{dh_0}{dr} = m_0 e^{4\lambda_0} \left(\frac{1}{r^2} + 8\pi p \right) - \frac{1}{12} e^{2\lambda_0} r^3 j^2 \left(\frac{d\varpi}{dr} \right)^2 + 4\pi r e^{2\lambda_0} (\epsilon + p) \delta p_0. \quad (32)$$

These equations will be integrated outward from the origin, where the boundary conditions $h_0(0) = m_0(0) = 0$ must be satisfied. In this approximation, the slowly rotating configuration will have the same central pressure as in the static case. In the exterior region, (31) and (32) can be integrated explicitly

$$m_0 = \delta M - \frac{J^2}{r^3}, \quad (33)$$

$$h_0 = -\frac{\delta M}{r - 2M_0} + \frac{J^2}{r^3 (r - 2M_0)}, \quad (34)$$

where M_0 corresponds to the total mass of the star and δM is an integration constant which is associated to the change in mass after the rotation. This constant δM can be found from the matching at the boundary $r = R$ of the interior and exterior solutions for h_0 .

The quadrupole deformations of the star are computed from the integrals of the $l = 2$ equations which gives

$$\frac{dv_2}{dr} = -2 \frac{dv_0}{dr} h_2 + \left(\frac{1}{r} + \frac{dv_0}{dr} \right) \left[\frac{1}{6} r^4 j^2 \left(\frac{d\varpi}{dr} \right)^2 - \frac{1}{3} r^3 \varpi^2 \frac{dj^2}{dr} \right], \quad (35)$$

$$\begin{aligned} \frac{dh_2}{dr} &= -\frac{2v_2}{r[r - 2m(r)](dv_0/dr)} \\ &+ \left\{ -2 \frac{dv_0}{dr} + \frac{r}{2[r - 2m(r)](dv_0/dr)} \left[8\pi(\epsilon + p) - \frac{4m(r)}{r^3} \right] \right\} h_2 \\ &+ \frac{1}{6} \left[r \frac{dv_0}{dr} - \frac{1}{2[r - 2m(r)](dv_0/dr)} \right] r^3 j^2 \left(\frac{d\varpi}{dr} \right)^2 \\ &- \frac{1}{3} \left[r \frac{dv_0}{dr} + \frac{1}{2[r - 2m(r)](dv_0/dr)} \right] r^2 \varpi^2 \frac{dj^2}{dr}, \quad (36) \end{aligned}$$

$$m_2 = [r - 2m(r)] \left\{ -h_2 - \frac{1}{3} r^3 \left(\frac{dj^2}{dr} \right) \varpi^2 + \frac{1}{6} r^4 j^2 \left(\frac{d\varpi}{dr} \right)^2 \right\} \quad (37)$$

where $v_2 = h_2 + k_2$. These equations will be integrated outward from the center, where $h_2 = v_2 = 0$. Outside the star, (35) and (36) are integrated analytically

$$h_2(r) = J^2 \left(\frac{1}{M_0 r^3} + \frac{1}{r^4} \right) + K Q_2^2 \left(\frac{r}{M_0} - 1 \right), \quad (38)$$

$$v_2(r) = -\frac{J^2}{r^4} + K \frac{2M_0}{[r(r - 2M_0)]^{1/2}} Q_2^1 \left(\frac{r}{M_0} - 1 \right), \quad (39)$$

where K is an integration constant which can be found from the continuity of the functions h_2, v_2 at the boundary, and Q_n^m are the associated Legendre functions of the second kind. The constant K in (38) and (39) is related to the quadrupole mass moment of the star, as measured at infinity, through the relation (Hartle & Thorne 1968)

$$Q = \frac{J^2}{M_0} + \frac{8}{5} K M_0^3. \quad (40)$$

4 STRUCTURE EQUATIONS FOR THE SCHWARZSCHILD STAR

In a seminal paper Chandrasekhar & Miller (1974) studied slowly rotating homogeneous masses using Hartle's framework. In that paper, the structure equations were integrated numerically and surface properties were computed for several values of the parameter R/R_s , where R is the radius of the star and R_s is the Schwarzschild radius. This procedure represented a quasi-stationary contraction of the star (Miller 1977). We will refer the relevant equations of that paper prefixed by the letters CM, for example (CM.1) indicates equation (1) of (Chandrasekhar & Miller 1974).

The geometry of the Schwarzschild star was discussed in 2. In order to facilitate the numerical integrations, it is useful to introduce the coordinates (CM.35)

$$r = (1 - y^2)^{1/2}, \quad y_1^2 = 1 - \frac{R^2}{a^2} = 1 - H^2 R^2. \quad (41)$$

Here r is being measured in the unit $\alpha = 1/H$, where H is given by (11). In terms of these variables the Schwarzschild star solution (6), (12), (13) and (14) takes the form

$$e^{\lambda_0} = \frac{1}{y}, \quad e^{v_0} = \frac{1}{2} |3y_1 - y|, \quad p = \frac{y - y_1}{3y_1 - y} \epsilon, \quad (42)$$

$$j = \frac{2y}{|3y_1 - y|}, \quad \frac{2m(r)}{r} = 1 - y^2. \quad (43)$$

Notice that in contrast to (CM.34), here we consider modulo of $(3y_1 - y)$ in (42) in harmony with the fact that the metric element

6 C. Posada-Aguirre

$e^{2\nu_0}$ in (14) is a perfect square making it always a positive quantity. Notice that the function e^{ν_0} is negative when $3y_1 < y$ which occurs in the region below the Buchdahl bound. Therefore, in order to investigate the region $R_s < R < (9/8)R_s$, it is important to specify the modulo condition. This specification was taken into account in the code to compute the numerical solutions. To facilitate computations, we define the quantity

$$k = |3y_1 - 1|, \quad (44)$$

which is always positive as it is required for the analysis of the region $R_s < R < (9/8)R_s$. It is also advantageous to introduce the coordinate (CM.39)

$$x \equiv 1 - y = 1 - \left[1 - \left(\frac{r}{a}\right)^2\right]^{1/2}, \quad (45)$$

where x covers the range $(0, 1 - y_1]$. In terms of (45), equation (25) reads

$$x \left[2k + (2 - k)x - x^2\right] \frac{d^2\varpi}{dx^2} + \left[5k + (3 - 5k)x - 4x^2\right] \frac{d\varpi}{dx} - 4(k + 1)\varpi = 0, \quad (46)$$

Near the origin ($x \approx 0$) ϖ satisfies

$$\varpi = \left[1 + \frac{4(k + 1)}{5k}x\right] \varpi_c \quad (47)$$

where ϖ is measured in the unit ϖ_c , its value at the center, which is arbitrary. The field equations (31), (32) take the forms

$$\frac{dm_0}{dx} = \alpha^3 \frac{(1 - x)[x(2 - x)]^{3/2}}{(k + x)^2} \left[\frac{1}{3}x(2 - x) \left(\frac{d\varpi}{dx}\right)^2 + \frac{8(k + 1)}{3(k + x)}\varpi^2 \right], \quad (48)$$

$$\begin{aligned} \frac{d}{dx} \delta P_0 = & -\frac{(k + 1)}{(1 - x)(k + x)} \delta P_0 \\ & - \left[\frac{2 + (k + 1)(1 - x) - 3(1 - x)^2}{(k + x)(1 - x)^2 [x(2 - x)]^{3/2}} \right] \alpha^{-1} m_0 + \frac{8x(2 - x)}{3(k + x)^2} \varpi \left(\frac{d\varpi}{dx}\right) \\ & + \frac{[x(2 - x)]^2}{3(1 - x)(k + x)^2} \left(\frac{d\varpi}{dx}\right)^2 - \frac{8}{3} \left[\frac{1 - (k + 1)(1 - x)}{(k + x)^3} \right] \varpi^2, \end{aligned} \quad (49)$$

which satisfy the near origin behaviors

$$m_0 = \left(\frac{32 \sqrt{2}(k + 1)}{15k^3} x^{5/2} \right) \alpha^3 \varpi_c^2, \quad (50)$$

$$\delta P_0 = \left(\frac{8x}{3k^2} \right) \alpha^2 \varpi_c^2. \quad (51)$$

The equations for h_2, v_2 as functions of x take now the form

$$\begin{aligned} \frac{dv_2}{dx} = & -\frac{2h_2}{k + x} \\ & + \alpha^2 \frac{2[x(2 - x)]^2}{3(k + x)^3} \left[1 + (k + 1)(1 - x) - 2(1 - x)^2 \right] \times \\ & \left[\left(\frac{d\varpi}{dx}\right)^2 + \frac{4(k + 1)}{x(2 - x)(k + x)} \varpi^2 \right], \end{aligned} \quad (52)$$

$$\begin{aligned} \frac{dh_2}{dx} = & \frac{(1 - x)^2 + (k + 1)(1 - x) - 2}{x(2 - x)(k + x)} h_2 - \frac{2(k + x)}{[x(2 - x)]^2} v_2 \\ & + \frac{\alpha^2}{3} \left\{ 2[x(2 - x)]^2 - (k + x)^2 \right\} \frac{x(2 - x)}{(k + x)^3} \left(\frac{d\varpi}{dx}\right)^2 \\ & + \frac{4\alpha^2}{3} (k + 1) \left[2x^2(2 - x)^2 + (k + x)^2 \right] \frac{\varpi^2}{(k + x)^4}. \end{aligned} \quad (53)$$

The functions $\delta P_0, \delta P_2, h_2, k_2$ and v_2 are measured in the unit $\alpha^2 \omega_c^2$ and m_0 is measured in the unit $\alpha^3 \omega_c^2$. Solutions to (52) and (53) can be expressed as the superposition of a particular and a complementary solution (CM.61)

$$h_2 = h_2^{(p)} + \beta h_2^{(c)}, \quad v_2 = v_2^{(p)} + \beta v_2^{(c)}, \quad (54)$$

with β an integration constant. The solutions to (54) satisfies the differential equations

$$\frac{dv_2^{(c)}}{dx} = -\frac{2h_2^{(c)}}{k + x}, \quad (55)$$

$$\begin{aligned} \frac{dh_2^{(c)}}{dx} = & \frac{(1 - x)^2 + (k + 1)(1 - x) - 2}{x(2 - x)(k + x)} h_2^{(c)} \\ & - \frac{2(k + x)}{[x(2 - x)]^2} v_2^{(c)}, \end{aligned} \quad (56)$$

which have the following near origin behaviors (CM.64)

$$h_2^{(p)} = cx, \quad v_2^{(p)} = ax^2, \quad (57)$$

$$h_2^{(c)} = -kBx, \quad v_2^{(c)} = Bx^2 \quad (58)$$

where $k^2(c + ka) = 8y_1$ and B is an arbitrary constant. On the other hand the exterior solutions (33),(34),(38) and (39) take the forms²

$$m_0 = \delta M - \frac{J^2}{r^3}, \quad h_0 = -\frac{m_0}{r - (1 - y_1^2)^{3/2}}, \quad (59)$$

$$h_2 = \left[\frac{2}{(1 - y_1^2)^{3/2}} + \frac{1}{r} \right] \frac{J^2}{r^3} + K Q_2^2, \quad (60)$$

$$v_2 = -\frac{J^2}{r^4} + K \frac{(1 - y_1^2)^{3/2}}{\left\{ r \left[r - (1 - y_1^2)^{3/2} \right] \right\}^{1/2}} Q_2^1. \quad (61)$$

At the boundary of the configuration, the interior equations (46)-(53) must match the exterior solutions (59)-(61). It can be observed that the structure equations preserve the same form as were considered in Chandrasekhar & Miller (1974). The only significant change corresponds to the modulo condition (44) which, we emphasize, is crucial to analyze the regime $R_s < R < 1.125R_s$.

5 RESULTS

In this section we present results of integrations of the Hartle structure equations and derived surface properties for a slowly rotating Schwarzschild star with negative pressure, in the unstudied regime $R_s < R < (9/8)R_s$. We followed similar methods to those used by Chandrasekhar & Miller (1974), in particular, units were chosen such that derived quantities are dimensionless. Similarly we constructed several configurations under quasi-stationary contraction, by varying the radius of the star through the parameter R/R_s . By convenience we introduce the ‘Schwarzschild deviation parameter’ $\zeta \equiv (R - R_s)/R_s$.

The integrations were performed numerically using the Runge-Kutta-Fehlberg (RKF) adaptive method in Python 3.4 (Kiusalaas 2010; Newman 2012). It is well known that adaptive

² There is a misprint in equation (CM.53), or equation (61) here. The numerator of the second term to the right should be $(1 - y_1^2)^{3/2}$.

methods are usually more convenient, than the standard fourth-order Runge-Kutta, when the function to be integrated changes rapidly near some point. In such situation, setting a constant step of integration h on the whole integration range might not be appropriate and we are forced to adjust the step to maintain the truncation error within prescribed limits. In our particular case, we found that the (RKF) method provided a fast, reliable and stable technique to integrate the structure equations near to and below the Buchdahl radius.

In our routine the condition (44) was specified which is key to analyze the region below the Buchdahl radius. We used the following values of the constant parameters: $\omega_c = 1.8$, $a = 1$, $B = 2$. However these values are arbitrary, therefore changing these would not alter the results of the surface properties. We have checked our code by reproducing the computations found in (Chandrasekhar & Miller 1974) for $R \geq 1.125R_s$. We found agreement up to the fourth decimal place in some cases (see Table 1). In contrast to CM paper, we are measuring the mass quadrupole moment Q in units of J^2/M_0 . It is useful to introduce the quantity (Bradley & Fodor 2009)

$$\frac{\Delta Q}{Q} \equiv \frac{Q - Q_{kerr}}{Q_{kerr}} \quad (62)$$

which corresponds to the relative deviation of the quadrupole moment from the Kerr metric value ($Q_{kerr} = J^2/M_0$).

One important observation by Chandrasekhar & Miller (1974) is that the structure equations can actually be integrated at the Buchdahl radius, i.e., $y_1 = 1/3$ and $k = 0$, by considering the expansions (CM.69)-(CM.71). We reproduced these results (see Table 1) with very good agreement, except for the mass quadrupole moment where we found $Q = 2.02311$ (in units of J^2/R_s). The fact that the structure equations are integrable at $R = (9/8)R_s$ might be seen as an early indication that the region below this limit is potentially interesting. This hypothesis has been investigated in this paper inspired in the results of Mazur & Mottola (2015). In the following, we present some plots of our results and further analysis.

In Fig. 4 we plot the angular velocity $\varpi(R)$ relative to the local ZAMO versus the ‘compactness parameter’ R/R_s , above the Buchdahl bound. Notice that $\varpi(R)$ reaches a maximum near to $R = 1.4R_s$ and then approaches to zero in the Newtonian limit $R \rightarrow \infty$. These results are in very good agreement with (Chandrasekhar & Miller 1974).

Figure 5 shows the angular velocity $\varpi(R)$ relative to the local ZAMO as a function of R/R_s in the regime $R_s < R < (9/8)R_s$. It is observed that in the limit when the radius of the star R approaches the Schwarzschild radius R_s , ϖ systematically decreases. For ζ of the order of 10^{-14} (gravastar limit), ϖ tends to zero. Therefore, in this limit, the angular velocity $\omega = \Omega$ is a constant indicating a *rigidly rotating body* with no differential surface rotation (Marsh 2014). Moreover, there is no frame-dragging at the boundary of the super-compact Schwarzschild star.

It can be shown that the value $\omega = \Omega = 2$ (in units of J/R_s^3) for the angular velocity of the super-compact Schwarzschild star in the gravastar limit ($\zeta \sim 10^{-14}$) is consistent with that of the Kerr black hole limit. It is well known that in the Kerr spacetime, a radially falling test particle with zero angular momentum acquires an angular velocity when it approaches the spinning black hole. The angular velocity as measured by a distant ZAMO is given by

$$\omega = \frac{d\phi}{dt} = \frac{2aM_0r}{(r^2 + a^2)^2 - \Delta(r)a^2 \sin^2 \theta}, \quad (63)$$

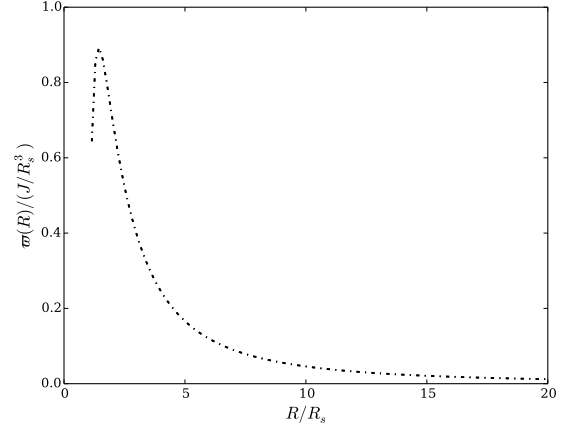


Figure 4. The angular velocity $\varpi = (\Omega - \omega)|_{r=R}$ (in units of J/R_s^3) relative to the local ZAMO, plotted as a function of the compactness parameter R/R_s above the Buchdahl-Bondi bound $R > 1.125R_s$.

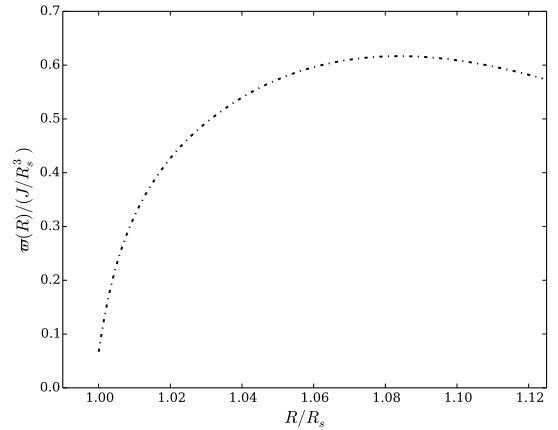


Figure 5. The angular velocity $\varpi = (\Omega - \omega)|_{r=R}$ (in units of J/R_s^3) relative to the local ZAMO, plotted as a function of the compactness parameter R/R_s in the region $R_s < R < 1.125R_s$.

where $a \equiv J/M_0$ and $\Delta(r) \equiv r^2 - 2M_0r + a^2$. Notice that positive a implies positive ω , therefore the particle will rotate in the spinning direction of the black hole. This is the so-called dragging effect in Kerr geometry. At the ‘event horizon’ (63) satisfies

$$\omega_{bh} = \frac{a}{2M_0r_+}, \quad (64)$$

where $r_+ = M_0 + (M_0^2 - a^2)^{1/2}$. Equation (64) corresponds to the angular velocity of the Kerr black hole. In the slowly rotating approximation ($\xi \equiv a/M_0 \ll 1$) a straightforward calculation from (64) shows that

$$\Omega = \omega_{bh} \approx \frac{a}{4M_0^2} + O(\xi^2) = 2 \left(\frac{J}{R_s^3} \right) + O(\xi^2) \quad (65)$$

which is consistent with our numerical results for Ω in the gravastar limit $\zeta \sim 10^{-14}$ (see Table 1).

From Fig. 6 can be observed that the normalized moment of inertia approaches the value 0.8 at the Buchdahl bound. For large values of R we notice that I_N tends to the value 0.4 which is the

Table 1. Integral and surface properties of a slowly rotating ‘Schwarzschild star’ for several values of the deviation parameter $\zeta \equiv \frac{R-R_s}{R_s}$, where R is the radius of the star and $R_s = 2M_0$ is the Schwarzschild radius. We use geometrized units ($c = G = 1$). The angular velocity relative to the local ZAMO $\varpi(R) = (\Omega - \omega)|_{r=R}$ is given in units of J/R_s^3 . The moment of inertia I is in the unit R_s^3 . The ratio $\delta M/M$ denotes the fractional change in mass, where δM is given by (33) and is measured in units of J^2/R_s^4 . The ratio $\Delta Q/Q$ defined in (62) corresponds to the relative deviation of the mass quadrupole moment from that of the Kerr metric. We measure the quadrupole moment Q in units of J^2/M_0 so the Kerr factor $\bar{q} = QM_0/J^2$ corresponds to the unity. All the quantities are computed at the surface of the configuration. The digit in parenthesis following each entry corresponds to the power of ten which the entry is multiplied.

ζ	$\varpi(R)$	Ω	I	$I_N = I/M_0R^2$	$\delta M/M$	$\Delta Q/Q$
99.0	4.958538 (-4)	4.978538 (-4)	2.008621 (+3)	4.017243 (-1)	9.950085 (-4)	6.093859 (+2)
49.0	1.966802 (-3)	1.982802 (-3)	5.043366 (+2)	4.034693 (-1)	3.960078 (-3)	2.970315 (+2)
34.0	3.984776 (-3)	4.031423 (-3)	2.480513 (+2)	4.049817 (-1)	8.046649 (-3)	2.033647 (+2)
9.0	4.582047 (-2)	4.782047 (-2)	2.091154 (+1)	4.182308 (-1)	9.493450 (-2)	4.794558 (+1)
7.0	6.994179 (-2)	7.384804 (-2)	1.354132 (+1)	4.231662 (-1)	1.463199 (-1)	3.575002 (+1)
4.0	1.662453 (-1)	1.822453 (-1)	5.487109 (0)	4.389687 (-1)	3.588505 (-1)	1.786438 (+1)
3.0	2.462305 (-1)	2.774805 (-1)	3.603856 (0)	4.504820 (-1)	5.439746 (-1)	1.217989 (+1)
2.0	3.969839 (-1)	4.710580 (-1)	2.122880 (0)	4.717512 (-1)	9.162061 (-1)	6.837185 (0)
1.0	7.029353 (-1)	9.529353 (-1)	1.049389 (0)	5.246945 (-1)	1.819485 (0)	2.263128 (0)
0.50	8.871430 (-1)	1.479735 (0)	6.757963 (-1)	6.007078 (-1)	2.756967 (0)	6.358729 (-1)
0.40	8.917486 (-1)	1.620611 (0)	6.170509 (-1)	6.296438 (-1)	2.992654 (0)	4.065443 (-1)
0.30	8.574163 (-1)	1.767748 (0)	5.656913 (-1)	6.694571 (-1)	3.224895 (0)	2.204677 (-1)
0.20	7.481799 (-1)	1.905587 (0)	5.247725 (-1)	7.288508 (-1)	3.412176 (0)	8.451602 (-2)
0.15	6.439067 (-1)	1.958939 (0)	5.104803 (-1)	7.719929 (-1)	3.454114 (0)	3.810123 (-2)
0.125	5.727118 (-1)	1.977375 (0)	5.057207 (-1)	7.991636 (-1)	3.442297 (0)	1.155989 (-2)
0.120	5.791167 (-1)	2.002677 (0)	4.993315 (-1)	7.961281 (-1)	3.323529 (0)	1.514229 (-2)
0.115	5.864895 (-1)	2.029287 (0)	4.927839 (-1)	7.927509 (-1)	3.194555 (0)	9.530643 (-3)
0.110	5.988341 (-1)	2.061216 (0)	4.851503 (-1)	7.875177 (-1)	3.013208 (0)	3.292989 (-3)
0.10	6.105343 (-1)	2.113163 (0)	4.732240 (-1)	7.821885 (-1)	2.775629 (0)	4.029515 (-3)
5.0 (-2)	5.733929 (-1)	2.301068 (0)	4.345807 (-1)	7.883551 (-1)	2.075953 (0)	9.936454 (-3)
1.0 (-2)	3.172159 (-1)	2.258396 (0)	4.427920 (-1)	8.681346 (-1)	1.984446 (0)	1.479216 (-3)
5.0 (-3)	2.326000 (-1)	2.202898 (0)	4.539473 (-1)	8.988834 (-1)	1.990433 (0)	6.408622 (-4)
1.0 (-3)	1.087716 (-1)	2.102783 (0)	4.755600 (-1)	9.492207 (-1)	1.997794 (0)	1.014025 (-4)
5.0 (-4)	7.770156 (-2)	2.074704 (0)	4.819963 (-1)	9.630294 (-1)	1.998875 (0)	4.752038 (-5)
1.0 (-4)	3.524386 (-2)	2.034643 (0)	4.914864 (-1)	9.827763 (-1)	1.999771 (0)	8.625562 (-6)
5.0 (-6)	7.967509 (-3)	2.007937 (0)	4.980234 (-1)	9.960369 (-1)	1.999988 (0)	3.986565 (-7)
1.0 (-6)	3.097802 (-3)	2.003091 (0)	4.992282 (-1)	9.984544 (-1)	1.999995 (0)	1.060546 (-7)
5.0 (-8)	6.925421 (-4)	2.000692 (0)	4.998269 (-1)	9.996538 (-1)	1.999999 (0)	5.287842 (-9)
1.0 (-12)	3.097088 (-6)	2.000003 (0)	4.999992 (-1)	9.999984 (-1)	2.0 (0)	1.056932 (-13)
1.0 (-14)	3.095711 (-7)	2.0 (0)	4.999999 (-1)	9.999998 (-1)	2.0 (0)	1.110223 (-15)

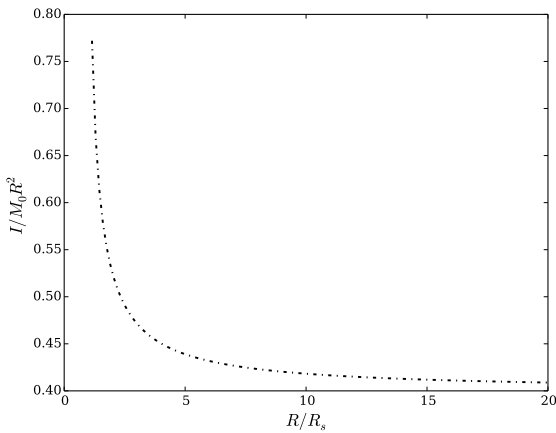


Figure 6. The normalized moment of inertia I_N plotted as a function of the compactness parameter R/R_s above the Buchdahl bound.

well known moment of inertia of a sphere in consistency with the Newtonian limit.

Figure 7 shows the normalized moment of inertia versus the factor R/R_s in the region $R_s < R < (9/8)R_s$. Notice the systematic approach to 1 of I_N when $R \rightarrow R_s^+$. This is in remarkable agreement with the Kerr value in the slowly rotating approximation

$$I = \frac{J}{\omega_{bh}} \approx 4M_0^3 + O(\xi^2). \quad (66)$$

In Fig. 8 is plotted the relative change of mass $\delta M/M_0$ as a function of the compactness parameter R/R_s , for $R \geq (9/8)R_s$. Notice the decrease in δM as we approach the Newtonian limit $R \rightarrow \infty$. On the other hand, Fig. 9 shows the fractional change in mass as a function of the parameter R/R_s in the region $R_s < R < (9/8)R_s$. Notice the systematic decrease of $\delta M/M_0$ for R below the Buchdahl bound, and its subsequent approach to the value 2 in the gravastar limit $R \rightarrow R_s^+$.

Finally in Fig. 10 the Kerr factor $\bar{q} = QM_0/J^2$ (Thorne 1971; Miller 1977) is plotted as a function of the parameter R/R_s . Notice the approach to the Kerr value $\bar{q} = 1$ when $R \rightarrow R_s^+$. A remarkable and unprecedented result is that relative deviations of the mass quadrupole moment as given by (62) are of the order of 10^{-15} in the gravastar limit $R \rightarrow R_s^+$ with $\zeta \sim 10^{-14}$. Therefore, we conclude that the exterior metric to a slowly rotating super-compact Schwarzschild star (with negative pressure) in the gravastar limit

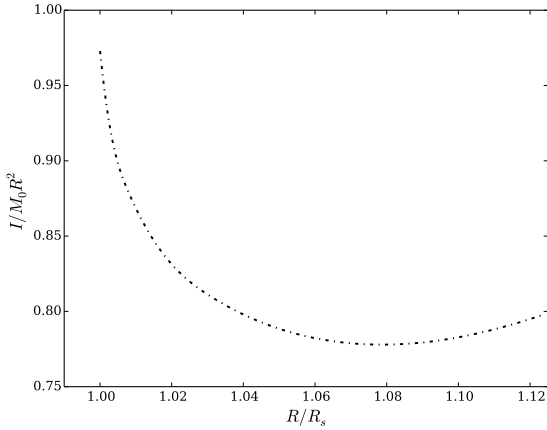


Figure 7. The normalized moment of inertia $I/M_0 R^2$ plotted as a function of the compactness parameter R/R_s in the region $R_s < R < 1.125R_s$. Notice the approach to 1 of the moment of inertia (normalized) in the gravastar limit $R \rightarrow R_s^+$.

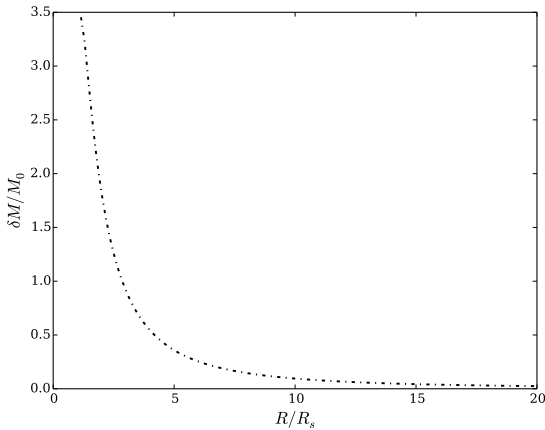


Figure 8. The fractional change of mass against the compactness parameter R/R_s above the Buchdahl bound.

$R \rightarrow R_s^+$, agrees to an accuracy of 1 part in 10^{15} with the Kerr metric.

6 CONCLUDING REMARKS

Motivated by recent investigations of Mazur & Mottola (2015) and the methods introduced by Hartle (1967) and Chandrasekhar & Miller (1974) in the study of slowly rotating relativistic masses, in this paper we have presented results of integral and surface properties for a slowly rotating super-compact Schwarzschild star in the unstudied regime $R_s < R < (9/8)R_s$. We found that the angular velocity ω relative to the local ZAMO tends to zero in the gravastar limit $R \rightarrow R_s^+$. This result indicates that the super-compact Schwarzschild star rotates rigidly with no differential surface rotation. Furthermore the angular velocity Ω of the super-compact Schwarzschild star, in the gravastar limit, is constant and approaches the corresponding Kerr value in the slowly rotating approximation.

Additionally, we found that the normalized moment of inertia

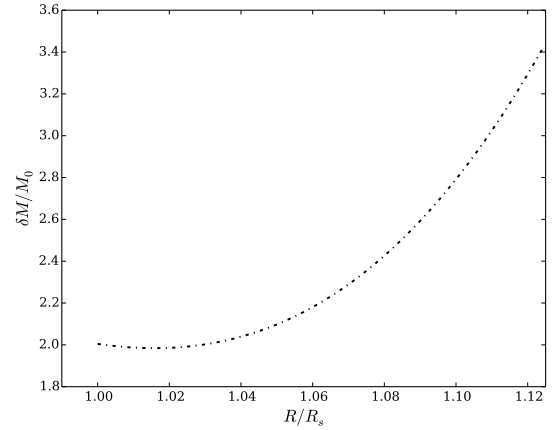


Figure 9. The fractional change of mass as a function of the compactness parameter R/R_s in the region $R_s < R < 1.125R_s$.

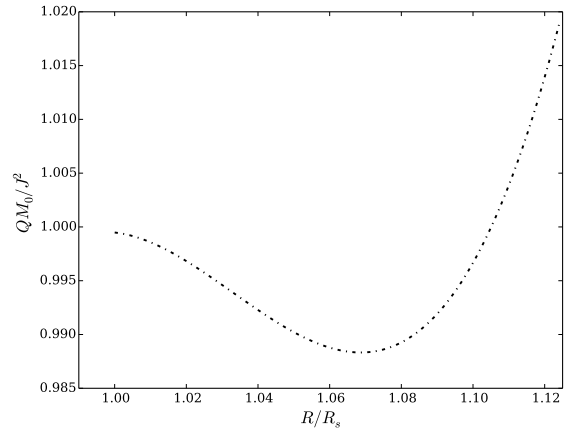


Figure 10. The Kerr factor $\bar{q} = Q M_0 / J^2$ plotted as a function of the compactness parameter R/R_s in the regime $R_s < R < (9/8)R_s$. Notice the approach to the Kerr value $\bar{q} = 1$ in the gravastar limit $R \rightarrow R_s^+$. In Table 1 it is shown that the relative deviation $\Delta Q/Q$ is of the order of 10^{-15} for $\zeta \sim 10^{-14}$.

$I/M_0 R^2$ approaches systematically to the unity when $R \rightarrow R_s^+$. This result is in agreement with the value corresponding to the slowly rotating Kerr metric. The most remarkable result concerns the mass quadrupole moment Q . We found that for a slowly rotating super-compact Schwarzschild star, in the gravastar limit, the relative deviation factor is $\Delta Q/Q \sim 10^{-15}$. These aforementioned results indicate that the external metric of a slowly rotating super-compact Schwarzschild star in the gravastar limit, agrees with the Kerr metric to the requisite order to one part in 10^{15} . These results provides the long-sought solution to the problem of the source of rotation of the slowly rotating Kerr metric.

ACKNOWLEDGEMENTS

I am grateful to Prof. Pawel O. Mazur for suggesting the problem and invaluable discussions. I would like to thank Dr. Timir Datta for reading the manuscript and important comments. I am indebted to Dr. Martin Urbanec and Prof. John C. Miller for useful suggestions

on the numerical part. Finally, I want to thank to the Department of Physics and Astronomy at USC where I was supported as a Teaching Assistant during this work.

REFERENCES

- Abramowicz M. A., Kluźniak W., Lasota J.-P., 2002, *A&A*, **396**, L31
 Bekenstein J. D., 1974, *Phys. Rev. D*, **9**, 3292
 Berezin V., 2003, *Nucl. Phys. B.*, **661**, 409
 Bradley M., Fodor G., 2009, *Phys. Rev. D*, **79**, 044018
 Buchdahl H. A., 1959, *Phys. Rev.*, **116**, 1027
 Chandrasekhar S., Miller J. C., 1974, *MNRAS*, **167**, 63
 Chapline G., 2001, *Phil. Mag. B.*, **81**, 235
 Chirenti C. B. M. H., Rezzolla L., 2007, *Class. Quantum Grav.*, **24**, 4191
 Frolov V. P., 2014, preprint, ([arXiv:1411.6981](https://arxiv.org/abs/1411.6981))
 Hartle J. B., 1967, *ApJ*, **150**, 1005
 Hartle J. B., Thorne K. S., 1968, *ApJ*, **153**, 807
 Hawking S. W., 1975, *Comm. Math. Phys.*, **43**, 199
 Hawking S. W., 1976, *Phys. Rev. D*, **14**, 2460
 Hawking S. W., 2014, preprint, ([arXiv:1401.5761](https://arxiv.org/abs/1401.5761))
 Horvat D., Iljić S., Marunović A., 2009, *Class. Quantum Grav.*, **26**, 025003
 Kiusalaas J., 2010, *Numerical Methods in Engineering with Python*, 2nd edn. Cambridge University Press
 Lobo F. S. N., 2006, *Class. Quantum Grav.*, **23**, 1525
 Marsh G. E., 2014, preprint, ([arXiv:1404.5297](https://arxiv.org/abs/1404.5297))
 Mazur P. O., Mottola E., 2001, preprint, ([arXiv:gr-qc/0109035](https://arxiv.org/abs/gr-qc/0109035))
 Mazur P. O., Mottola E., 2004, *Proc. Natl. Acad. Sci.*, **101**, 9545
 Mazur P. O., Mottola E., 2015, *Class. Quantum Grav.*, **32**, 215024
 Miller J. C., 1977, *MNRAS*, **179**, 483
 Misner C. W., Thorne K. S., Wheeler J. A., 1973, *Gravitation*. W. H. Freeman, San Francisco
 Mottola E., 2011, *Journal of Physics Conference Series*, **314**, 012010
 Narlikar J. V., 2010, *An Introduction to Relativity*. Cambridge University Press
 Newman M., 2012, *Computational Physics*. Createspace Independent Publishing
 Page D. N., 2005, *New J. Phys.*, **7**, 203
 Pani P., Berti E., Cardoso V., Chen Y., Norte R., 2009, *Phys. Rev. D*, **80**, 124047
 Schwarzschild K., 1916, *Sitzungsber. Preuss. Akad. Wiss. Phys. Math.*
 Stephens C. R., 't Hooft G., Whiting B. F., 1994, *Class. Quantum Grav.*, **11**, 621
 Stergioulas N., 2003, *Living. Rev. Relativity*, **6**
 Thorne K. S., 1971, in Sachs R. K., ed., *General Relativity and Cosmology*. Academic Press, pp 237–283
 Wald R. M., 1984, *General Relativity*. University of Chicago Press
 Wald R. M., 2001, *Living Rev. Relativity*, **4**

This paper has been typeset from a $\text{\TeX}/\text{\LaTeX}$ file prepared by the author.